

Meta-Backscatter: Long-Distance Battery-Free Metamaterial-Backscatter Sensing and Communication

Taorui Liu , Xu Liu , Zhiqian Xu , Houfeng Chen , Hongliang Zhang , Lingyang Song

Abstract— Battery-free Internet of Things (BF-IoT) enabled by backscatter communication is a rapidly evolving technology offering advantages of low cost, ultra-low power consumption, and robustness. However, the practical deployment of BF-IoT is significantly constrained by the limited communication range of common backscatter tags, which typically operate with a range of merely a few meters due to inherent round-trip path loss. Meta-backscatter systems that utilize metamaterial tags present a promising solution, retaining the inherent advantages of BF-IoT while breaking the critical communication range barrier. By leveraging densely paved sub-wavelength units to concentrate the reflected signal power, metamaterial tags enable a significant communication range extension over existing BF-IoT tags that employ omni-directional antennas. In this paper, we synthesize the principles and paradigms of metamaterial sensing to establish a unified design framework and a forward-looking research roadmap. Specifically, we first provide an overview of backscatter communication, encompassing its development history, working principles, and tag classification. We then introduce the design methodology for both metamaterial tags and their compatible transceivers. Moreover, we present the implementation of a meta-backscatter system prototype and report the experimental results based on it. Finally, we conclude by highlighting key challenges and outlining potential avenues for future research.

Keywords— meta-backscatter, metamaterial tags, battery-free Internet of Things, communication distance

1 Introduction

The Internet of Things (IoT) will serve as the core enabling technology for sixth-generation (6G) communications, supporting critical applications in healthcare, intelligent industry, and environmental protection^[1-2]. With projected tag deployments approximately ten times greater than current 5G networks^[3], 6G IoT systems demand tags that are low-cost, ultra-low power, and robust, i.e., capable of working in harsh environments for a long time without maintenance^[4]. However, conventional tags fail to meet these requirements due to their reliance on expensive and delicate electronic components such as transceivers, modulators, and processing units, combined with power-intensive battery systems that become unsustainable at scale^[5]. Therefore, realizing 6G IoT networks necessitates innovative tag architectures that fundamentally address these convergent challenges.

To address these limitations of traditional IoT tags, battery-free IoT (BF-IoT) tags have emerged, employing backscatter communication technology to eliminate internal power requirements^[6]. Rather than generating active transmissions, these devices modulate and reflect incident radio frequency signals toward transceivers^[7]. These devices encode data through controlled manipulation of load impedances, which alter scattering coefficients to modulate reflected signal amplitude and phase^[8]. This approach offers significant advantages: ultra-low power consumption at μ W levels, simplified architecture consisting only of antennas and radio control modules, manufacturing costs reduced to cents per unit, and operational lifespans exceeding ten years^[9]. The technology is particularly valuable for deployment in harsh environments where maintenance is impractical, including mining operations, chemical processing facilities, and embedded building infrastructure applications,

making backscatter tags an optimal solution for long-term, large-scale sensing networks in challenging conditions^[10]. This innovative approach thus represents a significant advancement in overcoming the fundamental constraints of traditional IoT tags.

Despite the numerous advantages of backscatter tags, due to the inherent round-trip path loss of backscatter communication, the communication range of backscatter tags is significantly shorter compared to traditional IoT devices^[11-12]. The typical communication range for common backscatter tags is only up to a few meters^[13-15], while the Third Generation Partnership Project (3GPP) requirements specify that IoT devices should achieve communication ranges exceeding 10-meter level. While some backscatter tags employing specially designed excitation signals, such as LoRa backscatter based on Chirp Spread Spectrum (CSS), can achieve a longer communication range, their power consumption is not low enough to support battery-free applications^[12]. This limited communication range significantly restricts the practical deployment of backscatter tags. To address the limitations of existing backscatter tags, metamaterial tags have been proposed. Specifically, metamaterial tags are sub-wavelength resonators combining environmentally sensitive structure that are periodically arranged on dielectric substrates^[16-17]. Unlike existing backscatter tags that typically employ omni-directional antennas with low directional gain^[18], the densely paved units with sub-wavelength spacing result in more concentrated reflected signal power and thus longer communication ranges, according to antenna theory^[19-20]. By combining the low cost, low power consumption, and high robustness of backscatter tags while overcoming communication range limitations, metamaterial tags demonstrate great potential for widespread applications^[21-22].

However, designing efficient sensing systems based on metamaterial tags, referred to as meta-backscatter systems, presents significant challenges due to the simultaneous sensing and transmission requirements. The frequency response characteristics of the tag critically influence both its sensing accuracy and communication performance^[23], and transmission effects cannot be disregarded during the sensing process^[24]. These aspects have been largely overlooked in existing reviews on backscatter communication^[7,11,25]. Moreover, current reviews on metamaterial tags^[22,26-29] have primarily focused on the design of sensing functionalities, often neglecting essential considerations related to the transmission process. Furthermore, they typically catalogue and summarize individual designs without proposing a comprehensive system framework that integrates tag design with custom transceiver implementation. Consequently,

establishing a unified framework for the co-design of sensing and communication is imperative.

Specifically, this work addresses the above gap by summarizing the fundamental principles, design paradigms, and key techniques specific to metamaterial sensing. Our main contributions are as follows:

- First, we present the fundamental principles of metamaterial tags and establish an equivalent circuit model to facilitate their design. A comprehensive review of existing tag designs further complements this theoretical groundwork.
- Next, we establish a signal sensing and transmission model for meta-backscatter systems. Based on this model, we analyze key signal detection techniques, highlighting their applicability and specific requirements.
- Furthermore, we implement a meta-backscatter system prototype and provide corresponding experimental results to demonstrate its practical feasibility.
- Finally, we outline the major research challenges and future directions, aiming to identify open problems and stimulate further investigation in this field.

The remainder of this paper is organized as follows. Section 2 provides an overview of backscatter communication, covering development history, fundamental principles, as well as tag category comparisons. Section 3 examines design principles, SRR-based circuit modeling, and a comprehensive literature review of metamaterial tags. Section 4 introduces a signal sensing and transmission model, followed by a discussion of key signal detection techniques. Section 5 presents the implementation of a meta-backscatter system prototype and corresponding experimental results. Section 6 identifies existing challenges and future research directions, while Section 7 concludes the paper.

2 Overview of Backscatter

This section begins with introduction of the development history of backscatter communication. Then we illustrate the fundamental principles of backscatter systems. Subsequently, we categorize backscatter tags by their signal modulation schemes and discuss their respective advantages and disadvantages.

2.1 Development History of Backscatter

The origins of backscatter communications can be traced to early radar systems used to detect the location of the enemy aircraft during World War II^[30]. In 1948, Harry Stockman published what is widely recognized as the first formal conceptualization of backscatter

communications in his landmark paper, “Communication by Means of Reflected Power”^[6], thereby establishing the theoretical foundation for subsequent developments in this field. Following this seminal work, backscatter communications continued to evolve along multiple research trajectories, ultimately culminating in the successful development of radio frequency identification (RFID) technology^[31]. The 1970s witnessed significant milestones, including the presentation of the earliest RFID prototype in patent form^[32] and a notable breakthrough by Los Alamos Scientific Laboratory, which developed an electronic identification system utilizing modulated backscatter waves from an ID tag^[33]. These developments marked the transition of backscatter communications from theoretical concept to practical reality.

As RFID technology matured, the first generation of backscatter tags emerged to eliminate battery dependence in wireless tags^[34-35]. In this typical configuration, conventional tags are integrated into RFID tags, enabling the backscattered signals to carry sensing data. Since these systems operate without batteries, both the RFID chip and tag rely on energy harvesting for power. However, in first-generation backscatter tags, the sensing and communication modules function independently. To fully exploit the inherent properties of backscatter communications, researchers developed second-generation electromagnetic RFID tags. Unlike their predecessors, these tags incorporate sensitive materials directly into the tag’s antenna rather than using conventional sensing components^[36]. The sensing data is directly encoded into the RFID tag’s electrical parameters, such as input impedance or antenna gain. This elimination of power-consuming tags significantly extends the effective operational range.

However, manufacturing and maintenance costs associated with chips remained a significant obstacle to widespread backscatter tag adoption. In the 2010s, third-generation chipless RFID tags emerged as a research focus due to their potential for reduced costs^[37-38]. These chipless RFID tags consist essentially of passive antennas or resonators that exhibit resonance frequencies sensitive to specific environmental targets, enabling sensing data to be extracted from the spectral characteristics of backscattered signals^[39-40]. This approach eliminates the need for digital circuits, relying solely on analog signal processing.

While offering cost advantages, chipless RFID tags suffer from limited accuracy and operational range, constraining their practical deployment. To address these challenges, a novel chipless technique utilizing metamaterial tags has been proposed^[21]. These tags feature specialized resonant elements arranged in periodic two-

dimensional arrays to achieve enhanced sensitivity and improved backscatter beam gain. Consequently, metamaterial tags enable long-range sensing without power consumption, representing a promising solution for passive Internet of Things applications.

2.2 Fundamentals of Backscatter

A backscatter communication system consists of two primary components: transceivers and tags. The transceiver transmits excitation signals within a specific frequency band and receives scattered signals from tags. The tag modulates its scattering coefficient based on the sensing information to be transmitted, thereby altering the scattered signal. The operation of a backscatter communication system involves three sequential steps: forward transmission, tag scattering, and backward reception. First, transmitters such as WiFi hotspot or cellular base stations emit wireless excitation signals. Second, the tag adjusts its scattering coefficient according to the sensing information, thereby modifying the scattered signal. Finally, the receiver estimates the tag’s scattering coefficient from the received scattered signal to infer the tag’s sensing information.

Specifically, scattered signals S_{out} encode sensing information through variations in amplitude or phase:

$$S_{\text{out}} = |S_{\text{in}}| |\Gamma_{\text{tag}}| e^{i(2\pi f_{\text{in}} t + \theta_{\text{in}} + \theta_{\text{tag}})}, \quad (1)$$

where $|S_{\text{in}}|$ and θ_{in} denote the amplitude and phase of the excitation signal, f_{in} denotes the frequency of the excitation signal, and $|\Gamma_{\text{tag}}|$ and θ_{tag} denotes the amplitude and phase of the tag’s scattering coefficient. Based on whether the scattering coefficient exhibits discrete or continuous variations, tags can be classified as digital or analog types, which will be discussed in the following.

2.3 Classification of Backscatter Tags

2.3.1 Digital Backscatter Tags

As illustrated in Fig. 1(a), a digital backscatter tag comprises four key components: a peripheral tag, a signal control module, a radio frequency (RF) antenna, and a power supply (either battery or energy harvesting module). The peripheral tag detects environmental information and converts them into a binary bit stream, which is then transmitted to the signal control module. This module consists of RF switches and an impedance network, where the binary bit stream from the tag controls the switching states of the RF switches, effectively connecting the RF antenna to different load impedances. The impedance matching or mismatching

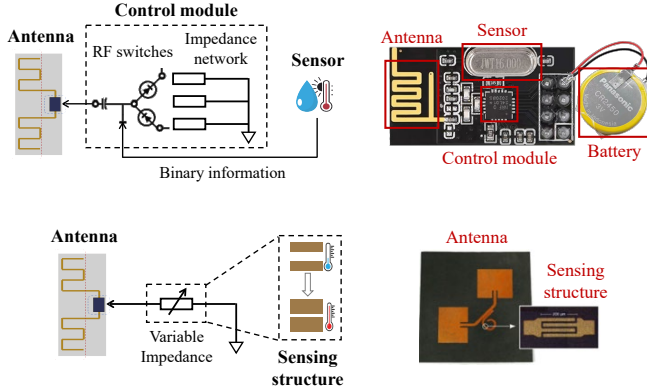


Figure 1 (a) A digital backscatter tag. (b) An analog backscatter tag.

between the antenna and load alters the tag's scattering coefficient, enabling data modulation onto the incident RF signal. Through appropriate demodulation techniques, the transceiver can successfully recover the transmitted sensing data. The power supply module provides the necessary energy for all operational processes. The switchable impedance values of the network are limited, consequently, the variation of the scattering coefficients is also discrete.

Various commercially available chip-based RFID tags fall under the category of digital backscatter tags. Due to the superior interference resistance of digital modulated signals, digital tags can achieve higher sensing accuracy^[41]. However, energy harvesting modules typically provide power only in the microwatt range^[42], while size-constrained batteries employ ultra-thin designs that cannot sustain high power consumption over extended periods. Consequently, digital tags can accommodate only a limited variety of tags and support basic sensing functions such as temperature or light intensity monitoring^[34-35]. Furthermore, the delicate microchips in digital tags may incur prohibitive maintenance costs in harsh environmental conditions or during large-scale deployments^[25,43].

2.3.2 Analog Backscatter Tags

Unlike digital tags, analog tags consist solely of an RF antenna and an electromagnetic resonant structure, as shown in Fig. 1(b). During measurement, the transceiver transmits a frequency sweep signal. The electromagnetic resonant structure resonates with the incident signal, absorbing signals at specific frequency points. As the environmental parameters being sensed change, the impedance of the electromagnetic resonator structure varies accordingly, causing shifts in the absorption frequency points. The transceiver then extracts sensing

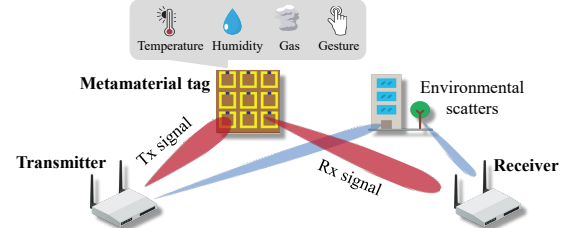


Figure 2 The illustration of a meta-backscatter system.

information from the scattered signal spectrum. Since the impedance of the resonant structure changes continuously with environmental variations, the scattering coefficient also varies continuously.

Chipless RFID tags are among the most widely studied analog tags. The sensing capability of analog tags is achieved through electromagnetic resonant structures without requiring batteries or energy harvesting, thereby enabling support for a wider range of sensing functions, including strain monitoring, humidity monitoring, gas concentration detection, or gesture recognition^[44-47]. Furthermore, analog tags feature simple structures without delicate microchips, resulting in lower production and maintenance costs^[48]. However, analog-modulated signals are susceptible to channel noise interference, resulting in limited sensing accuracy^[41].

The replacement of the omni-directional antenna in existing backscatter tags with a metamaterial array enables a substantial extension of communication range and, crucially, provides support for both digital and analog modulations. Owing to this unique design philosophy, the discussion in subsequent sections will focus on issues pertaining to analog metamaterial tags.

3 Metamaterial Tag Design

This section begins by elucidating the design principles of metamaterial tags. Subsequently, we present the equivalent circuit model, using split-ring resonator (SRR) as an example, which is one of the most prevalent metamaterial structures. The section concludes with an overview of metamaterial designs from related works.

3.1 Design Principles

Fig. 2 illustrates the composition of a meta-backscatter system. As discussed in the previous section, metamaterial tags enable simultaneous sensing and transmission through frequency-selective reflection of signals based on their structural design. This operational principle necessitates an approach to design metamaterial tags, requiring joint consideration of sensing and

transmission performance^[23]. Specifically, the sensing accuracy is intrinsically linked to variations in reflected signals across different tag states, while the tag structure significantly influences the intensity of received signals, thereby affecting the overall transmission range. Furthermore, the metamaterial structure incorporates multiple parameters, influencing the tag performance jointly^[24]. Consequently, the optimal tag design necessitates a comprehensive evaluation of all relevant structural parameters to identify the most effective configuration within a vast domain of feasible options.

To address the aforementioned challenges, we propose a multi-objective optimization framework for metamaterial structures. This framework aims to enhance two critical aspects of system performance: sensing accuracy and transmission range. By striking a balance between these objectives, the framework seeks to achieve optimal overall functionality. Sensing accuracy, primarily dependent on the tag's sensitivity, is quantified through measurable changes in the reflected signal. The sensing principle of metamaterial relies on their resonant frequency's sensitivity to specific targets due to the presence of sensitive materials^[16], and information about sensing targets can be obtained by measuring the resonant frequency of reflected signals^[44]. Consequently, a larger frequency shift generally indicates higher sensing accuracy^[45]. The Q-factor, or quality factor, is a dimensionless parameter characterizing the efficiency of a resonant system^[49]. A higher Q-factor signifies a lower rate of energy loss relative to stored energy, implying more efficient and sharper resonance. At equal resonance frequency shifts, a higher Q-factor results in more distinguishable changes in the reflected signal, thereby enhancing sensing accuracy^[50]. For these reasons, this study adopts resonance frequency shift and Q-factor as metrics for sensing accuracy.

Concurrently, the transmission range is evaluated using the signal-to-noise ratio (SNR), which requires careful consideration of the reflected signal's intensity. While some researchers have used change gradient in reflected power^[23,51] or average reflected power^[21] to measure transmission range, we employ the minimum reflected power over the frequency band. A higher minimum reflected power corresponds to a higher minimum SNR over the frequency band, thus enabling a longer transmission range^[19]. Besides, to simplify the multi-parameter optimization, we utilize equivalent circuit model, which is discussed in detail in the subsequent section.

3.2 Equivalent Circuit Model

The metamaterial structure incorporates numerous design parameters, including unit cell geometry, spacing,

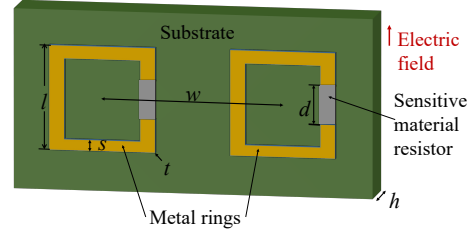


Figure 3 SRR particles.

and material composition, all of which collectively determine the tag's frequency response, as discussed in the previous section. Attempting to optimize all these parameters simultaneously would result in prohibitive computational complexity, rendering the process impractical. To address this challenge, a frequency response model based on an equivalent circuit has been proposed, striking a balance between computational efficiency and modeling precision^[52]. This approach simplifies the metamaterial tag structure by representing it as a limited number of circuit components, allowing for more manageable analysis. By projecting parameter changes onto these circuit components, the model intuitively demonstrates their impact on the overall frequency response. The optimization process is further streamlined through the classification of parameters and the selection of those deemed essential^[53]. Consequently, this methodology significantly reduces the feasible set for optimization, making the process more tractable and efficient while maintaining a high degree of accuracy in modeling the frequency response.

Split-ring resonators (SRRs) are among the most frequently utilized metamaterial tag structures due to their ease of design and fabrication^[26]. As shown in Fig. 3, the structural dimensions of the SRR particle can be described as follows: We use l to denote the side length of the ring, d to denote the width of the gap, s to denote the width of the ring, w to denote the distance between the centers of adjacent SRR particles, t to represent the thickness of the ring, and h to denote the thickness of the substrate. It is worth noticing that the direction of the gap is aligned vertically, and the direction of the electric field is parallel to the gap. Using SRRs as an example, we present the proposed equivalent circuit model and provide insight for metamaterial tag design based on this model in the following.

3.2.1 Overview of model

The layout of the investigated metamaterial tag structure and its corresponding equivalent circuit are illustrated in Fig. 4. The structure comprises SRRs with environmentally sensitive material resistors straddling their

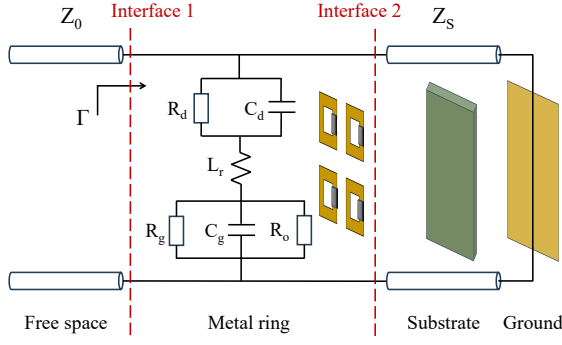


Figure 4 Equivalent circuit model.

gaps, periodically arranged on a lossy grounded dielectric substrate. The SRRs on the upper surface are analogous to a two-port circuit network, while the substrate and metal ground on the reverse side are equivalent to a terminated short-circuited transmission line. According to transmission line theory, the scattering coefficient Γ of the metamaterial tag, can be calculated as^[54]:

$$\Gamma = \frac{Z_{\text{tag}}(f, \psi_{\text{env}}) - Z_0}{Z_{\text{tag}}(f, \psi_{\text{env}}) + Z_0}, \quad (2)$$

where $Z_0 = 377 \Omega$ is equivalent impedance for free-space transmission^[54], ψ_{env} denotes the environmental parameter to be sensed, and Z_{tag} is equivalent impedance of the metamaterial tag, i.e., impedance from interface 1 to the right as shown in Fig. 4. Based on derivations in^[54], we can prove that Z_{tag} is equal to the parallel connection of Z_{SRR} and Z_S , where Z_{SRR} is the total impedance of the RLC circuit between interfaces 1 and 2, Z_S is impedance of the terminated short-circuited transmission line from interface 2 to the right as shown in Fig. 4.

3.2.2 Circuit components

Next, we focus on the the RLC circuit between interfaces 1 and 2 as shown in Fig. 4. In the presented RLC circuit, C_d is the dielectric capacitor, R_d denotes the dielectric resistor, L_r denotes the metal ring inductor, C_g is the gap capacitor, R_g is the gap resistor, and R_o denotes the ohmic resistor. These equivalent circuit parameters are described as follows:

C_d represents the capacitance formed between adjacent SRRs. As each SRR is surrounded by four others, C_d can be expressed as a series connection of four capacitors^[55], such that $C_d = C_0/4$, where C_0 denotes the capacitance between two neighboring SRRs and can be modeled as described in^[55]. Similarly, C_g denotes the capacitance formed at the gap of the metal ring, which can be calculated using the same method as C_0 .

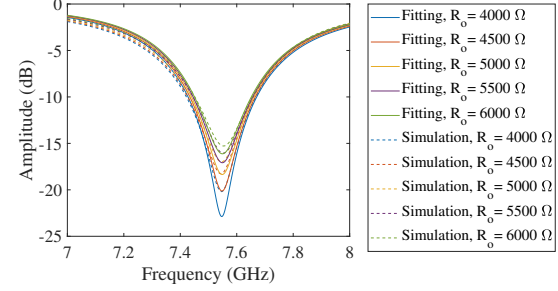


Figure 5 Comparison between simulated results and fitting results with different sensitive material resistance R_o .

The imaginary component of the substrate's relative dielectric constant introduces a resistive element that accounts for the effect of the lossy substrate in proximity to the metal rings. This loss component can be represented by a resistor R_d in parallel with the lossless capacitor C_d , and a resistor R_g in parallel with the lossless capacitor C_g ^[52].

L_r represents the inductance formed by the metal ring, which can be modeled based on the method described in^[56]. The value of R_o corresponds to the resistance of the sensitive material resistors.

3.2.3 Discussions based on circuit model

Consider the above RLC circuit in parallel with the substrate impedance Z_S . Let R_{total} , L_{total} , and C_{total} represent the total resistance, inductance, and capacitance, respectively. Then the resonant frequency f_0 can be expressed as $1/2\pi\sqrt{L_{\text{total}}C_{\text{total}}}$ ^[57]. The Q-factor can be modeled based on the equivalent circuit model, as described in^[58]:

$$Q = \frac{1}{R_{\text{total}}} \sqrt{\frac{L_{\text{total}}}{C_{\text{total}}}}. \quad (3)$$

The absorption peak depth is determined by the minimum amplitude of scattering coefficient Γ_{\min} , which can be calculated as:

$$\Gamma_{\min} = \left| \frac{Z_0 - R_{\text{total}}}{Z_0 + R_{\text{total}}} \right|. \quad (4)$$

Fig. 5 compares simulated results with equivalent circuit model fitting results for varying sensitive material resistance R_o . As R_o increases, R_{total} increases correspondingly, resulting in a lower Q-factor. Additionally, equation (4) indicates that Γ_{\min} is minimized when $R_{\text{total}} = Z_0$. Consequently, as R_o increases, Γ_{\min} initially decreases and subsequently increases.

Fig. 6 presents a comparison between simulated results and equivalent circuit model fitting results for different gap widths d . An increase in d leads to a decrease in

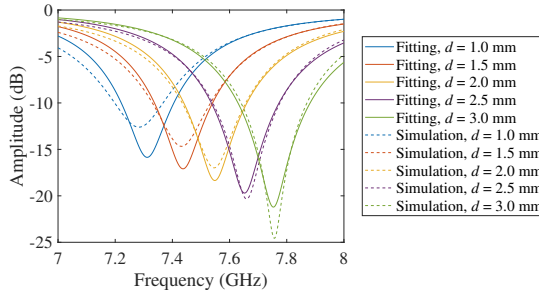


Figure 6 Comparison between simulated results and fitting results with different gap width d .

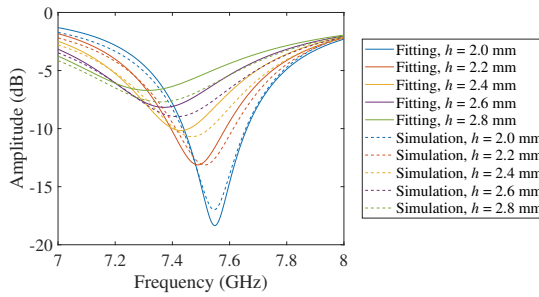


Figure 7 Comparison between simulated results and fitting results with different substrate thickness h .

C_{total} ^[55], consequently reducing C_{total} . This results in a higher resonant frequency and an increased Q-factor.

Fig. 7 illustrates the comparison between simulated results and equivalent circuit model fitting results for varying substrate thickness h . The substrate impedance Z_S is a complex value with inductive and resistive components^[52]. As h increases, Z_S increases accordingly, leading to an increase in L_{total} and a consequent decrease in resonant frequency. Furthermore, the increase in h results in a higher R_{total} , leading to a lower Q-factor.

Fig. 8 shows the comparison between simulated results and equivalent circuit model fitting results for different ring widths s . An increase in s leads to a decrease in L_r , as the average value of the inner and outer ring diameters decreases^[56]. This results in a decrease in L_{total} , leading to a higher resonant frequency and a lower Q-factor.

Based on the above discussion, The performance of an SRR is governed by the following design rules:

- Operating Frequency: Increased with a larger gap width d , a thinner substrate h , or a wider ring width s .
- Q-factor: Enhanced by a larger gap width d , a thinner substrate h , or a narrower ring width s .
- Absorption Peak Depth: Primarily determined by selecting a sensitive material with an optimal sheet resistance R_o .

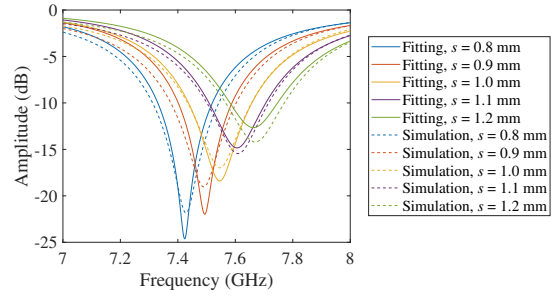


Figure 8 Comparison between simulated results and fitting results with different ring width s .

3.3 Other Tag Designs

Various studies have proposed alternative tag designs to achieve specific application objectives beyond the most common configurations. Several researchers have focused on modifying the metal structure's shape to attain desired electromagnetic properties. For instance, researchers found that the coupling capacitance between inner and outer ring in edge-coupled SRRs leads to lower resonance frequency, making them more suitable for low frequency applications^[59]. Similarly, a nested SRR design was introduced where numerous gaps in the structure significantly increase equivalent capacitance, thereby reducing resonance frequency for low frequency applications^[60]. It has also been demonstrated that broadside-coupled SRRs are less sensitive to the polarization of incident electromagnetic waves compared to standard SRRs, making them more convenient for deployment^[61]. Other researchers have also specially designed the metal structure to sense specific targets. For example, a series of dipoles in different orientations was utilized for angular rotation monitoring^[62], while SRR with a cantilever at the gap was adopted for strain sensing^[63].

Another approach is to focused on designing the substrate. Some researchers have chosen specialized substrate materials to sense specific targets. For instance, ceramic^[48] for temperature sensing, polyvinyl alcohol^[64] and hydrogel^[65] for humidity sensing. Some researchers focus on structures of the substrate. Researchers employed a multi-layer substrate, incorporating a sensing medium with environmentally sensitive permittivity between two common substrate layers to enhance sensing capabilities^[66]. Furthermore, a Kirigami structure was designed on a flexible substrate, leveraging its ability to transform one-dimensional strains into three-dimensional rotations, thereby improving strain sensitivity^[67].

Researchers have also incorporated tunable components into tag structure to achieve tunability^[68], particularly for multi-band operations. One approach involves

Table 1 List of Other Related Metamaterial Tag Design

Reference	Tag Feature	Design Objective
Ref. [59]	Edge-coupled SRR	Coupling capacitance between the inner and outer ring in edge-coupled SRRs leads to lower resonance frequency, making them more suitable for low frequency applications
Ref. [60]	Nested SRR	Numerous gaps in the nested structure significantly increase equivalent capacitance, thereby reducing resonance frequency for low frequency application
Ref. [61]	Broadside-coupled SRR	Broadside-coupled SRRs exhibit superior isotropy compared to standard SRRs for normally incident electromagnetic waves, making them more suitable for polarization-independent applications
Ref. [62]	Dipole	A series of dipoles in different orientations provides sensitivity for angular rotation monitoring
Ref. [63]	SRR with a cantilever at the gap	A sensing medium with environmentally sensitive permittivity is incorporated between two common substrate layers to enhance sensing capabilities
Ref. [66]	Multi-layer substrate	Incorporating a sensing medium with environmentally sensitive permittivity between two common substrate layers to enhance sensing capabilities
Ref. [67]	Flexible substrate of Kirigami structure	The Kirigami structure transforms one-dimensional strains into three-dimensional rotations, thereby improving strain sensitivity
Ref. [69]	Varactor diode placed on the gap of SRR	Changing the bias voltage changes the impedance in the equivalent circuit, resulting in changes in structure's operating band
Ref. [70]	SRR with adjustable inner ring-substrate distance	By adjusting inner ring-substrate distance using MEMS, structure's operating band is tunable over a wide frequency range

strategically placing tunable electronic elements within the tag. For instance, varactor diodes were mounted on the gap of SRR^[69]. By altering the bias voltage of these varactor diodes, the impedance in the equivalent circuit changes, resulting in shifts in the tag's operating band. Another approach involves mechanically adjusting the position or orientation of tag's fractions. An edge-coupled SRR was designed with an adjustable inner ring-substrate distance^[70]. By modifying this distance using MEMS, the structure's operating band can be tuned across a wide frequency range.

4 Signal Transmission and Detection

In the previous sections, we discussed the basic concepts of backscatter tags and their design principles. However, sensing and transmission occur simultaneously in this system, creating interdependent challenges. First, the sensing tag design affects both sensing and transmission capabilities through its frequency response characteristics. Second, transmission effects must be considered during the sensing process. Consequently, extracting sensing information from wireless signals remains an open research problem. In this section, we first introduce a signal sensing and transmission model for metamaterial tags. Based on this model, we then discuss key techniques for signal detection.

4.1 Signal and Interference Model

The backscatter system is composed of two components, i.e., multiple metamaterial tags and a multi-antenna wireless transceiver i.e. Tx and Rx. In such a system, the Tx and Rx have line-of-sight (LOS) paths to the i -th metamaterial tag and can be analysis by the Friis' free-space link model^[71]:

$$P_{\text{rec},i}(f, \psi_{\text{env}}) = \frac{P_{\text{Tx}} \sigma \lambda^2}{32\pi^3 r_{\text{Tx},i}^2 r_{\text{Rx},i}^2} \cdot \Gamma^2(f, \psi_{\text{env},i}) \cdot G_{\text{Tx},i} \cdot G_{\text{Rx},i}, \quad (5)$$

where P_{Tx} denotes transmit power, σ denotes the area of a metamaterial tag, f is the frequency of the incident signal, $r_{\text{Tx},i}$, $r_{\text{Rx},i}$ are the distance between Tx or Rx antenna array and the i -th tag, $\Gamma(f, \psi_{\text{env},i})$ indicates the scattering coefficient of the i -th tag defined in 2, λ is the wavelength of the incident signal, and $G_{\text{Tx},i}$, $G_{\text{Rx},i}$ is the gain factor of the Tx or Rx antenna array in direction of the i -th tag, respectively.

In the system, the transmitted signals are not only reflected by the target tag but also by other tags and environmental scatters. Considering the total number of tags to be I , the interference received during measurement of the i -th metamaterial sensing tag can be be expressed as:

$$P_{\text{inf},i}(f, \psi_{\text{env}}) = \sum_{j \in [1, I]}^{j \neq i} \frac{P_{\text{Tx}} \sigma \lambda^2}{32\pi^3 r_{\text{Tx},j}^2 r_{\text{Rx},j}^2} \cdot \Gamma^2(f, \psi_{\text{env},j}) \cdot G_{\text{Tx},j} \cdot G_{\text{Rx},j} + \eta \cdot P_{\text{Tx}} \cdot \Gamma_{\text{env},i}, \quad (6)$$

where the first part in the expression is due to the signals reflected by other tags while the second part is due to ambient scattering.

4.2 Signal Detection Methods

From the transceiver perspective, the special simultaneous transmission and sensing of a meta-backscatter system requires specialized signal processing methods. The sensing principle of metamaterial tags relies on frequency response variations of individual tags. However, during transmission, the signal is affected not only by the tag's frequency response but also by variable and complex wireless channel conditions, as described in signal and interference model. Unlike conventional tags that separate sensing and transmission functions using linear and explicit transfer functions, meta-backscatter system requires transfer functions that account for wireless channel effects, necessitating sophisticated signal processing approaches. There are two main categories of solutions: traditional signal processing methods and deep learning methods.

4.2.1 Traditional signal detection methods

Traditional signal detection methods can be classified as either calibrated or uncalibrated, based on their requirement for background normalization—a process involving the subtraction of empty measurements from tag measurements. Calibrated methods rely on the Singularity Expansion Method (SEM)^[72], which is premised on the fact that an object's electromagnetic response is fully characterized by singularities in the complex frequency plane. These singularities are independent of various transmission parameters but depend solely on the scattering tag's properties^[73]. Thus, sensing information can be separated from the transmitted signal by extracting these singularities. Specifically, the Matrix Pencil Method (MPM)^[74] and its variant, the Short-Time Matrix Pencil Method (STMPM)^[75], were developed for this purpose.

However, in practical scenarios involving rapidly varying background clutter, accurate background normalization becomes considerably difficult to achieve. Instead of relying on background subtraction, uncalibrated methods focus on disentangling the overlapped components within the composite backscattered signal in the time, frequency, or time-frequency domain. For instance, a time-gating algorithm was introduced to detect a tag based on a co-polar patch resonator integrated with delay stubs^[76]. Similarly, a joint time-domain and frequency-domain (TD-FD) analysis was presented to ef-

fectively separate the individual contributions within the backscattered signal^[77]. Expanding on time-frequency analysis, a method utilizing the short-time Fourier transform (STFT) was proposed for improved tag detection^[78]. Furthermore, a mathematical model was developed to precisely extract the tag's information from the raw signal^[79]. These methods collectively demonstrate the potential of signal processing techniques in directly isolating tag responses under challenging conditions.

4.2.2 Deep learning methods

Deep learning methods offer another promising solution due to their capacity to model complex relationships with large datasets^[80]. Specifically, deep learning approaches extract critical features from signals through data-driven learning and map these features to sensing outcomes^[81]. From a network architecture perspective, these models capture wireless channel effects through extensive received signal analysis, enabling sensing results to be derived from interference-corrupted signals.

Deep learning methods can be categorized into two approaches: supervised and unsupervised learning. Supervised learning requires labeled training data containing signal measurements and their corresponding ground-truth sensing results to train the network as a transfer function, thereby achieving precise quantitative sensing outputs from input signals. For instance, Convolutional Neural Networks (CNNs)^[82] are based on local connectivity and weight-sharing, while Recurrent Neural Networks (RNNs)^[83] and Long Short-Term Memory (LSTM) networks^[84] model temporal dependencies for sequential signal processing. Conversely, unsupervised learning identifies patterns and distinctions within unlabeled measurement signals without explicitly optimizing for precise results through predefined transfer functions. Unsupervised learning employs various approaches, ranging from Autoencoders^[85] that discover structures by reconstructing inputs to generative models like RBMs^[86], DBNs^[87], and GANs^[88], which learn data distributions or create new samples.

Deep learning methods offer a distinct advantage over traditional approaches in highly complex and dynamic wireless environments where explicit channel modeling is challenging due to their ability to disentangle tag responses from severe interference^[89]. This advantage comes with two main challenges: substantial data requirements and high computational complexity. Deep learning methods necessitates large, diverse, and accurately datasets for training, which requires in-situ data collection and labeling after deployment. Moreover, the real-time processing of signals from a massive number

of tags places a substantial computational burden on the transceiver, where the deep learning algorithms are typically deployed. This scalability challenge necessitates research into cloud-edge collaborative network architectures to achieve efficient allocation of computational tasks between cloud servers and transceivers.

Several studies have applied deep learning techniques to metamaterial sensing signal detection. An unsupervised deep learning algorithm was developed that processes received signals and outputs anomaly detection and localization indicators to effectively mitigate impairments from wireless transmission^[24]. An end-to-end signal processing framework was proposed utilizing deep learning algorithms to extract key signal features, such as resonance frequency and Q-factor, for sensing result determination^[21]. Deep learning was employed for joint channel estimation and signal demodulation to address signal distortion caused by variable frequency responses of tags^[90]. These deep learning approaches significantly enhance the signal processing capabilities and information extraction performance of meta-backscatter systems.

5 Implementation and Prototype

In this section, the implementation of a meta-backscatter system prototype are presented, along with experimental results. The prototype metamaterial tag was designed following the principles in Section 3. In the prototype transceiver, we use the introduced signal processing method in Section 4 as an example.

5.1 Metamaterial Tag Implementation

The metamaterial unit is composed of the top-metal patterns, the substrate, and the metal ground. as shown in Fig. 9, the top-metal patterns are designed based on the SRR structure whose sizes are $10.09 \times 10.09 \times 2.4$ mm³, filling the gap with sensitive material. The gap of of metamaterial units is filled with hygristor TELAiRE HS30P (humidity-sensitive material) to sense environmental humidity. The tag units are designed with specific structure parameters and an absorption peak located around 5.25 GHz.

5.2 Transceiver platform implementation

5.2.1 Transceiver

The transceiver comprises Tx/Rx antennas and RF devices controlled by a Raspberry Pi.

- **Tx/Rx Antennas:** The Tx/Rx antennas are composed of a waveguide-to-coax adapter (159WCAS) and a

rectangular waveguide (159WAL-50) from A-INFO.

- **Radio-Frequency (RF) Switches:** To reduce the number of RF chains needed in the wireless transceiver, we adopt two RF switches to multiplex single Tx and Rx chains. Specifically, the 8 Tx antennas are connected to a single- pole-8-throw RF switch (HMC 321), and the 2 Rx antennas are connected to a single-pole-2-throw RF switch (HMC 270).

- **Low Noise Amplifiers (LNA):** The poles of the two RF switches are connected to the ports of two LNAs (ZX-6043-S+), which can provide an average gain of about 13.5 dB at [5.0,5.5] GHz to amplify the transmitted signals.

5.2.2 Signal analyzer

We employed a USRP hardware platform (NI; X410) to construct the transceiver and provide flexible signal processing including signal waveform, filtering, and basic digital analogue conversion. The transmitter was configured to emit a FMCW signal, while the receiver was set up to down-convert and sampling the backscattered signals. The FMCW signal is defined by the LabVIEW software in USRP with period of $1e^{-5}$ s and bandwidth of 200MHz in the based band.

5.2.3 Data processor

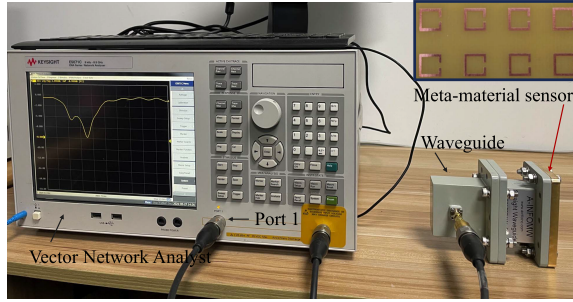
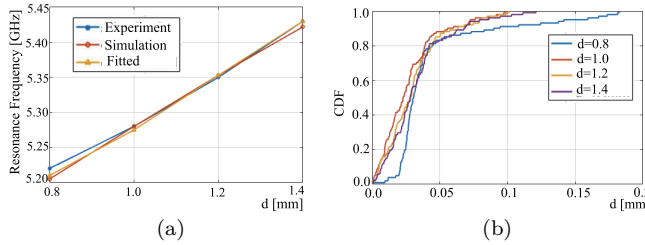
A host computer is connected to the Raspberry Pi and signal analyzer through an ethernet switch. The software program written in Python is used to control and communicate with them. A real time signal pretreatment method runs on the host computer performing the signal filtering, time-frequency transformation and basic tag detection algorithm. Besides, the signal processing algorithm is written in Python with Tensorflow 2.6 framework.

5.3 Measurement and Results

The measurement environment is designed to evaluate the performance of the meta-backscatter system in terms of the tag's sensing sensitivity. The experimental setting and results are shown as following:

5.3.1 Metamaterial tag sensing sensitivity

In this experiment, we fabricated metamaterial tags using the structural parameters defined in Section 3 with varying gap widths and measured their scattering coefficients in a waveguide test environment, as shown in Fig. 9. The waveguide environment is a widely adopted

Figure 9 The waveguide measurement scenario^[71].Figure 10 (a) Resonance frequencies of fitted, simulated, and experimental scattering coefficients of the metamaterial tags with different gap widths. (b) Cumulative distribution function of the difference between fitted and experimental results^[71].

method for measuring the frequency response of microwave tags, as it confines microwave energy propagation to a single direction within a specified frequency range. Scattering coefficient measurements were performed using a square waveguide (WR159) connected to the port of a vector network analyzer (VNA) (Agilent E5071C) configured for S_{11} parameter measurement.

Specifically, we characterized metamaterial tags with gap widths of 0.8, 1.0, 1.2, and 1.4 mm, with results presented in Fig. 10. As demonstrated in Fig. 10(a), the resonance frequency increases with increasing gap width d , consistent with the theoretical predictions described in Section 3. Furthermore, the maximum deviation in resonance frequency among fitted, simulated, and experimental results is less than 0.015 GHz. The cumulative distribution function shown in Fig. 10(b) reveals an average Euclidean distance of approximately 0.0438 between fitted and experimental results. These results validate the effectiveness of the proposed equivalent circuit model for optimizing metamaterial structures.

5.3.2 Prototype meta-backscatter system

The prototype system was evaluated in a typical indoor environment to demonstrate humidity distribution estimation on a wall surface, as illustrated in Fig. 11. Specifically, The sensing area covers a $2\text{ m} \times 2\text{ m}$ surface discretized into a 4×4 grids. Humidity levels ranging

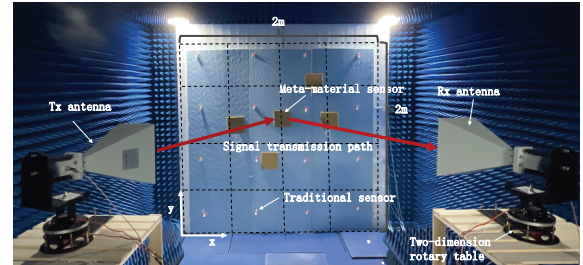
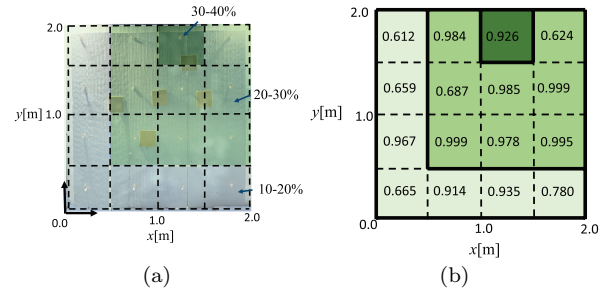
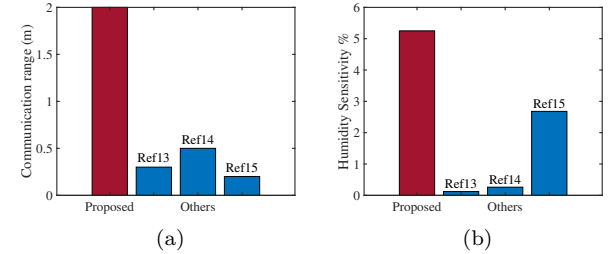
Figure 11 The experimental setting scenario^[71].Figure 12 (a) The humidity category of each space grid. (b) The estimated probability for the correct category^[71].

Figure 13 Comparison between the proposed meta-backscatter system with existing works. (a) Communication range. (b) Sensing sensitivity.

from 0% to 100% were categorized into 10 discrete intervals of 10% each. To generate controlled humidity distributions, water-retaining materials with varying moisture content were strategically positioned across the test surface. We adopted a deep learning method based on the preceding bidirectional recurrent network to realize the perception of environmental distribution.

Fig. 12 presents representative experimental results for the 4×4 spatial grids. Fig. 12(a) illustrates the measured humidity distribution across the grid points, while Fig. 12(b) displays the classification confidence calculated by the reconstruction algorithm. These experimental results demonstrate that the proposed meta-backscatter system exhibits high-precision capabilities for humidity distribution detection. The comparison of the communication range and sensing sensitivity with ex-

Table 2 Comparison of the Proposed System with Existing Works

Reference	Frequency Band	Test Environment	Sensor Scale	Deployment	Transmission Range	Sensitivity
Proposed	5.0-5.5 GHz	Indoor environment	$10.09 \times 10.09 \text{ mm}^2$	Sensor array	2.0 m	5.25%
Ref. [13]	6.5-9.0 GHz	Air-tight chamber	$15.0 \times 6.8 \text{ mm}^2$	Single sensor	0.3 m	0.12%
Ref. [14]	3.0-4.0 GHz	Anechoic chamber	$40.0 \times 40.0 \text{ mm}^2$	Single sensor	0.5 m	0.26%
Ref. [15]	2.6-3.0 GHz	Waveguide	$30.0 \times 19.0 \text{ mm}^2$	Single sensor	0.2 m	2.68%

isting backscatter tags is presented in Fig. 13(a) and 13(b). A detailed comparison of the measurement setups is listed in Table 2. It is shown that the proposed meta-backscatter system has higher sensitivities and achieves at least a 4-fold transmission range compared with the existing works. Moreover, experiments confirm that the system is capable of detecting humidity anomalies over a maximum distance of 10 meters, significantly outperforming existing schemes confined to decimeter-level ranges.

6 Challenges and Open Questions

Although metamaterial tags represent a promising approach for backscatter communication, realizing their full potential requires addressing several key challenges. This section examines three critical aspects: beamforming design in transmitters, multi-tag networking implementation, and the utilization of existing communication signals for integrated sensing and communication. By analyzing these challenges and discussing potential solutions alongside open research questions, we establish a roadmap for advancing metamaterial sensing research and maximizing its transformative impact on BF-IoT systems.

6.1 Transmitter Beamforming

Generally, a transmitter equipped with beamforming capability can concentrate signal power toward the target tag to maintain adequate signal to-noise ratio (SNR), thereby reducing interference. However, the transmitter faces a fundamental constraint: metamaterial tags operate in passive mode and cannot provide feedback to assist channel estimation. Given this physical limitation, the transmitter must employ an iterative transmission approach to achieve precise sensing results. The process operates as follows: First, the transmitter sends a signal that is received and processed to generate a sensing result, which is then fed back to the transmitter along with the received signal characteristics. Second, the transmitter analyzes both the received signal and sensing result to estimate channel conditions and designs an optimized sig-

nal spectrum for subsequent transmission. Finally, using the derived signal spectrum and estimated channel conditions, a broadband beamforming algorithm calculates a new beam direction, initiating the next transmission cycle.

6.2 Multi-tag Networking

As the demand for IoT sensing continues to grow, deploying multiple tags in a target area to acquire high-resolution environmental information becomes increasingly essential. However, simultaneous sensing with multiple tags introduces several challenges. When multiple tags are active simultaneously, their backscatter signals overlap at the receiver, potentially causing significant interference, which may degrade overall system performance. Additionally, since meta-backscatter systems operate in the frequency domain, traditional time-division multiple access (TDMA)-based protocols for identification are not suitable, making it difficult to distinguish the contributions of individual tags to the received signal. These issues are particularly problematic in dense deployments, where the number of tags increases significantly. To mitigate interference and enable effective networking, it is crucial to develop effective interference management strategies for multi-tag networks, thus ensuring accurate sensing and identification of each tag. To enable effective multi-tag identification, a joint time-frequency domain analysis framework was proposed to mitigate interference in multi-tag scenarios^[91]. A joint time-frequency domain detection algorithm is developed to enhance identification accuracy. Additionally, the authors analyzed the error probability of multi-tag identification and found that there exists an optimal transmission power that maximizes energy efficiency.

Although notable progress has been made in multi-tag networking, several challenges remain unaddressed. First, existing networking protocols lack adaptive access capabilities. Since tag access depends on the reader's excitation signals, the management of newly joining tags remains unresolved. How to design a dynamic access protocol that can dynamically adjust frequency-domain resource allocation to cope with environmental uncertain-

ties remains an open problem. In addition, existing studies primarily assume static environments. In practical applications, however, tag mobility and environmental variations may lead to the dynamic changes in interference characteristics, which makes the static models unreliable. Developing adaptive interference models that can account for such dynamics remains an open problem.

6.3 Integrated Sensing and Communication Design

As discussed in the previous sections, metamaterial tags encode the sensing information into their frequency response, which is then captured by the transceiver via signal reflection. Simultaneously, by functioning as environmental scatterers, metamaterial tags hold the potential to provide additional paths for existing communication systems, thereby enhancing the communication performance^[92]. Consequently, this dual functionality establishes a win-win Integrated Sensing and Communication (ISAC) paradigm. Different from traditional ISAC systems that primarily limited to radar-based sensing of geometric and movement characteristics^[93], the metamaterial tag-enabled system supports diverse sensing functionalities for ISAC. In addition, the ISAC paradigm significantly reduces the extensive bandwidth and hardware requirements of metamaterial tags through the efficient reuse of existing communication system resources.

However, the integration of sensing and communication introduces a fundamental trade-off between sensing accuracy and communication performance, which are inherently constrained by limited resources, including hardware capabilities, available spectrum, and energy budgets. To effectively address this challenge and realize the full potential of metamaterial tag-enabled ISAC systems, a comprehensive joint optimization framework is essential. This framework must encompass three critical design domains: the structural configuration of metamaterial tags, transmitter waveforming and beamforming strategies, and receiver signal processing algorithms, all of which must be jointly designed to balance the competing demands of sensing and communication objectives^[90].

6.4 Manufacturability and Deployability

Printed Circuit Board (PCB) technology presents an ideal solution for the large-scale manufacture of metamaterial tags, as their structure essentially comprises periodic metallic patterns printed on dielectric substrates. This compatibility, coupled with low material requirements, allows the use of low-cost standard materials,

such as copper-clad FR-4 substrates. Additionally, the environmentally sensitive structure can be implemented using thermistors, hygrometers, or photoresistors combined with Surface Mount Technology (SMT). Leveraging fundamental PCB processes, the unit cost of individual metamaterial tags can be reduced to just a few cents. Furthermore, their flat, passive design makes them exceptionally suitable for integration into building structures like walls and floor slabs. Once embedded during construction, these tags can function as building structural monitors throughout the building phase and continue to provide long-term environmental monitoring thereafter. Moreover, once deployed within a fixed operational environment, the tags can undergo a one-time calibration. This initial sampling and reference setup ensure consistent and reliable long-term measurements without the need for recurrent adjustments.

7 Conclusion

This survey has systematically articulated the unique position and design considerations of metamaterial tags within the BF-IoT landscape. Unlike existing BF-IoT devices, metamaterial tags offer significantly extended communication range, yet they introduce the fundamental challenge of jointly designing coupled sensing and transmission functions. To address this core complexity, this work has consolidated the underlying principles, design methodologies, and implementation techniques into a unified framework, providing a much-needed synthesis of this fragmented field. Our prototype experiments demonstrated the effectiveness of meta-backscatter systems for accuracy environmental monitoring while significantly extending the communication range. Finally, we discussed the key challenges and open research directions, including beamforming, networking, and ISAC design. The potential of metamaterial tags to unlock new frontiers in BF-IoT is evident. As research advances, we expect them to mature into a key enabling technology for building pervasive and intelligent sensing networks.

Conflict of interest statement. None declared.

References

- [1] HASSAN W H, et al. Current research on Internet of Things (IoT) security: A survey[J]. Computer Networks, 2019, 148(15): 283-294.
- [2] XIONG Z, ZHANG Y, LUONG N C, et al. The best of both worlds: A general architecture for

data management in blockchain-enabled Internet-of-Things[J]. *IEEE Network*, 2020, 34(1): 166-173.

[3] ZHANG S, ZHANG H, SONG L. Beyond D2D: Full dimension UAV-to-everything communications in 6G[J]. *IEEE Transactions on Vehicular Technology*, 2020, 69(6): 6592-6602.

[4] WIKSTRÖM G, PEISA J, RUGELAND P, et al. Challenges and technologies for 6G[C]//Proceedings of IEEE 6G Wireless Summit (6G SUMMIT). Piscataway: IEEE Press, 2020: 1-5.

[5] AL-TURJMAN F. Editorial: Potential sensors for the forthcoming 6G/IoE-electronics and physical communication aspects[J]. *Mobile Networks and Applications*, 2021, 26(3): 949-951.

[6] STOCKMAN H. Communication by means of reflected power[J]. *Proceedings of the IRE*, 1948, 36(10): 1196-1204.

[7] XU C, YANG L, ZHANG P. Practical backscatter communication systems for battery-free internet of things: A tutorial and survey of recent research[J]. *IEEE Signal Processing Magazine*, 2018, 35(5): 16-27.

[8] VOUGIOUKAS G, BLETSAS A. Switching frequency techniques for universal ambient backscatter networking[J]. *IEEE Journal on Selected Areas in Communications*, 2019, 37(2): 464-477.

[9] VULLERS R J, VAN SCHAIJK R, VISSER H J, et al. Energy harvesting for autonomous wireless sensor networks[J]. *IEEE Solid-State Circuits Magazine*, 2010, 2(2): 29-38.

[10] MAHESWARI D U, SUDHA S, MEENALOCHANI M. Fuzzy based adaptive clustering to improve the lifetime of wireless sensor network[J]. *China Communications*, 2019, 16(12): 56-71.

[11] JIANG T, ZHANG Y, MA W, et al. Backscatter communication meets practical battery-free Internet of Things: A survey and outlook[J]. *IEEE Communications Surveys & Tutorials*, 2023, 25(3): 2021-2051.

[12] TALLA V, HESSAR M, KELLOGG B, et al. LoRa backscatter: Enabling the vision of ubiquitous connectivity[J]. *Proceedings of the ACM on interactive, mobile, wearable and ubiquitous technologies*, 2017, 1(3): 1-24.

[13] AMIN E M, BHUIYAN S, KARMAKAR N, et al. A novel EM barcode for humidity sensing[C]//2013 IEEE International Conference on RFID. Piscataway: IEEE Press, 2013: 82-87.

[14] DENG F, HE Y, LI B, et al. Design of a slotted chipless RFID humidity sensor tag[J]. *Sensors and Actuators B: Chemical*, 2018, 264: 255-262.

[15] EKMEKCI E, KOSE U, CINAR A, et al. The use of metamaterial type double-sided resonator structures in humidity and concentration sensing applications [J]. *Sensors and Actuators A: Physical*, 2019, 297: 111559.

[16] CUI T J, SMITH D R, LIU R. *Metamaterials: Theory, design, and applications*[M]. Boston, MA, USA: Springer, 2010.

[17] LIU Y, ZHANG X. Metamaterials: a new frontier of science and technology[J]. *Chemical Society Reviews*, 2011, 40(5): 2494-2507.

[18] AHSON S A, ILYAS M. *RFID handbook: applications, technology, security, and privacy*[M]. Boca Raton, FL, USA: CRC press, 2008.

[19] GOLDSMITH A. *Wireless communications*[M]. Cambridge, UK: Cambridge Univ. Press, 2005.

[20] DI B, ZHANG H, HAN Z, et al. Reconfigurable holographic surface: A new paradigm for ultra-massive MIMO[J]. *IEEE Transactions on Cognitive Communications and Networking*, 2025.

[21] LIU X, HU J, ZHANG H, et al. Internet of metamaterial things: A new paradigm for passive wireless sensing systems[J]. *IEEE Communications Magazine*, 2024, 62(4): 136-142.

[22] XU W, XIE L, YING Y. Mechanisms and applications of terahertz metamaterial sensing: a review[J]. *Nanoscale*, 2017, 9(37): 13864-13878.

[23] HU J, ZHANG H, DI B, et al. Meta-IoT: Simultaneous sensing and transmission by meta-material sensor based Internet of Things[J]. *IEEE Transactions on Wireless Communications*, 2022, 21(8): 6048-6063.

[24] HU J, ZHANG H, DI B, et al. Meta-material sensor based Internet of Things: Design, optimization, and implementation[J]. *IEEE Transactions on Communications*, 2022, 70(8): 5645-5662.

[25] REZAEI F, TELLAMBURA C, HERATH S. Large-scale wireless-powered networks with backscatter communications—a comprehensive survey[J]. *IEEE Open Journal of Communications Society*, 2020, 1: 1100-1130.

[26] PRAKASH D, GUPTA N. Applications of metamaterial sensors: a review[J]. *International Journal of Microwave and Wireless Technologies*, 2022, 14(1): 19-33.

[27] CHEN T, LI S, SUN H. Metamaterials application in sensing[J]. *Sensors*, 2012, 12(3): 2742-2765.

[28] MAYANI M G, HERRAIZ-MARTÍNEZ F J, DOMINGO J M, et al. Resonator-based microwave metamaterial sensors for instrumentation: Survey, classification, and performance comparison[J]. *IEEE Transactions on Instrumentation and Measurement*, 2020, 70: 1-14.

[29] SALIM A, LIM S. Review of recent metamaterial microfluidic sensors[J]. *Sensors*, 2018, 18(1): 232.

[30] DOBKIN D. The RF in RFID: UHF RFID in practice[M]. Oxford, UK: Newnes, 2012.

[31] LANDT J. The history of RFID[J]. *IEEE Potentials*, 2005, 24(4): 8-11.

[32] CARDULLO M, PARKS W. Transponder apparatus and system: US3713148A[P]. 1973-01-23.

[33] KOELLE A R, DEPP S W, FREYMAN R W. Short-range radio-telemetry for electronic identification, using modulated RF backscatter[J]. *Proceedings of the IEEE*, 1975, 63(8): 1260-1261.

[34] CHO N, SONG S J, KIM S, et al. A 5.1- μ W UHF RFID tag chip integrated with sensors for wireless environmental monitoring[C]//Proceedings of the 31st European Solid-State Circuits Conference. Piscataway: IEEE Press, 2005: 279-282.

[35] OPASJUMRUSKIT K, THANTHIPWAN T, SATHUSEN O, et al. Self-powered wireless temperature sensors exploit RFID technology[J]. *IEEE Pervasive Computing*, 2006, 5(1): 54-61.

[36] MARROCCO G. Pervasive electromagnetics: sensing paradigms by passive RFID technology[J]. *IEEE Wireless Communications*, 2010, 17(6): 10-17.

[37] PRERADOVIC S, BALBIN I, KARMAKAR N C, et al. Multiresonator-based chipless RFID system for low-cost item tracking[J]. *IEEE Transactions on Microwave Theory and Techniques*, 2009, 57(5): 1411-1419.

[38] DEY S, SAHA J K, KARMAKAR N C. Smart sensing: Chipless RFID solutions for the internet of everything[J]. *IEEE Microwave Magazine*, 2015, 16 (10): 26-39.

[39] HERROJO C, PAREDES F, MATA-CONTRERAS J, et al. Chipless-RFID: A review and recent developments[J]. *Sensors*, 2019, 19(15): 3385.

[40] COSTA F, GENOVESI S, BORGESE M, et al. A review of RFID sensors, the new frontier of internet of things[J]. *Sensors*, 2021, 21(9): 3138.

[41] HAYES M H. Statistical digital signal processing and modeling[M]. Hoboken, NJ, USA: Wiley, 1996.

[42] KARTHAUS U, FISCHER M. Fully integrated passive UHF RFID transponder IC with 16.7- μ w minimum RF input power[J]. *IEEE Journal of Solid-State Circuits*, 2003, 38(10): 1602-1608.

[43] YUAN Y, ZHAO Y, ZONG B, et al. Potential key technologies for 6G mobile communications[J]. *Science China Information Sciences*, 2020, 63: 1-19.

[44] MELIK R, UNAL E, PERKGOZ N K, et al. Metamaterial-based wireless strain sensors[J]. *Applied Physics Letters*, 2009, 95(1).

[45] BORGESE M, DICANDIA F A, COSTA F, et al. An inkjet printed chipless RFID sensor for wireless humidity monitoring[J]. *IEEE Sensors Journal*, 2017, 17(15): 4699-4707.

[46] VENA A, SYDÄNHEIMO L, TENTZERIS M M, et al. A fully inkjet-printed wireless and chipless sensor for CO₂ and temperature detection[J]. *IEEE Sensors Journal*, 2015, 15(1): 89-99.

[47] ASADZADEH P, KULIK L, TANIN E. Gesture recognition using rfid technology[J]. *Personal and Ubiquitous Computing*, 2012, 16(3): 225-234.

[48] KAIRM H, DELFIN D, SHUVO M A I, et al. Concept and model of a metamaterial-based passive wireless temperature sensor for harsh environment applications[J]. *IEEE Sensors Journal*, 2014, 15(3): 1445-1452.

[49] COLLIN R E. Field theory of guided waves[M]. Hoboken, NJ, USA: Wiley, 1990.

[50] ZHU H, ZHANG Y, YE L, et al. A high Q-factor metamaterial absorber and its refractive index sensing characteristics[J]. *IEEE Transactions on Microwave Theory and Techniques*, 2022, 70(12): 5383-5391.

[51] LIU T, HU J, ZHANG H, et al. Beyond Specular Reflector: Broadening Reflection Coverage for Internet of Meta-material Things[J]. *IEEE Transactions on Wireless Communications*, 2024, 23(7): 7924-7937.

[52] COSTA F, GENOVESI S, MONORCHIO A, et al. A circuit-based model for the interpretation of perfect metamaterial absorbers[J]. *IEEE Transactions on Antennas and Propagation*, 2012, 61(3): 1201-1209.

[53] ZENG S, ZHANG H, DI B, et al. Intelligent omni-surfaces: Reflection-refraction circuit model, full-dimensional beamforming, and system implementation[J]. *IEEE Transactions on Communications*, 2022, 70(11): 7711-7727.

[54] POZAR D M. *Microwave engineering*[M]. Hoboken, NJ, USA: Wiley, 2005.

[55] BILOTTI F, TOSCANO A, VEGNI L, et al. Equivalent-circuit models for the design of metamaterials based on artificial magnetic inclusions[J]. *IEEE Transactions on Microwave Theory and Techniques*, 2007, 55(12): 2865-2873.

[56] MOHAN S S, DEL MAR HERSHENSON M, BOYD S P, et al. Simple accurate expressions for planar spiral inductances[J]. *IEEE Journal of Solid-State Circuits*, 1999, 34(10): 1419-1424.

[57] COSTA F, MONORCHIO A, MANARA G. Efficient analysis of frequency-selective surfaces by a simple equivalent-circuit model[J]. *IEEE Antennas and Propagation Magazine*, 2012, 54(4): 35-48.

[58] BRIZI D, FONTANA N, COSTA F, et al. Accurate extraction of equivalent circuit parameters of spiral resonators for the design of metamaterials[J]. *IEEE Transactions on Microwave Theory and Techniques*, 2019, 67(2): 626-633.

[59] SUN R, LI W, MENG T, et al. Design and optimization of terahertz metamaterial sensor with high sensing performance[J]. *Optics Communications*, 2021, 494: 127051.

[60] MELIK R, UNAL E, PERKGOZ N K, et al. Nested metamaterials for wireless strain sensing[J]. *IEEE Journal of Selected Topics in Quantum Electronics*, 2009, 16(2): 450-458.

[61] MARQUÉS R, MESA F, MARTEL J, et al. Comparative analysis of edge- and broadside-coupled split ring resonators for metamaterial design-theory and experiments[J]. *IEEE Transactions on Antennas and Propagation*, 2003, 51(10): 2572-2581.

[62] GENOVESI S, COSTA F, BORGESE M, et al. Chipless radio frequency identification (RFID) sensor for angular rotation monitoring[J]. *Technologies*, 2018, 6(3): 61.

[63] THAI T T, AUBERT H, PONS P, et al. Novel design of a highly sensitive RF strain transducer for passive and remote sensing in two dimensions [J]. *IEEE Transactions on Microwave Theory and Techniques*, 2013, 61(3): 1385-1396.

[64] AMIN E M, KARMAKAR N C, WINTHERR-JENSEN B. Polyvinyl-alcohol (PVA)-based RF humidity sensor in microwave frequency[J]. *Progress In Electromagnetics Research*, 2013, 54: 149-166.

[65] DAUTTA M, ALSHETAIWI M, ESCOBAR A, et al. Multi-functional hydrogel-interlayer RF/NFC resonators as a versatile platform for passive and wireless biosensing[J]. *Advanced Electronic Materials*, 2020, 6(4): 1901311.

[66] EKMEKCI E, TURHAN-SAYAN G. Multi-functional metamaterial sensor based on a broadside coupled srr topology with a multi-layer substrate[J]. *Applied Physics A*, 2013, 110: 189-197.

[67] DIJVEJIN Z A, KAZEMI K K, ALAS-VAND ZARASVAND K, et al. Kirigami-enabled microwave resonator arrays for wireless, flexible, passive strain sensing[J]. *ACS Applied Materials & Interfaces*, 2020, 12(39): 44256-44264.

[68] TURPIN J P, BOSSARD J A, MORGAN K L, et al. Reconfigurable and tunable metamaterials: a review of the theory and applications[J]. *International Journal of Antennas and Propagation*, 2014, 2014(1): 429837.

[69] BAKIR M, KARAASLAN M, DINÇER F, et al. Tunable perfect metamaterial absorber and sensor applications[J]. *Journal of Materials Science: Materials in Electronics*, 2016, 27: 12091-12099.

[70] YANG J, LIN Y S. Design of tunable terahertz metamaterial sensor with single-and dual-resonance characteristic[J]. *Nanomaterials*, 2021, 11(9): 2212.

[71] LIU X, HU J, ZHANG H, et al. Meta-material sensor based internet of things for environmental monitoring by deep learning: Design, deployment, and implementation[J]. *IEEE Transactions on Wireless Communications*, 2023, 22(4): 2462-2476.

[72] BAUM C E. On the singularity expansion method for the solution of electromagnetic interaction problems[R]. 1971.

[73] MITTRA R, BAUM C E, SENGUPTA D, et al. Transient electromagnetic fields[M]. Boston, MA, USA: Springer, 2006.

[74] SARKAR T K, PEREIRA O. Using the matrix pencil method to estimate the parameters of a sum of complex exponentials[J]. IEEE Antennas and Propagation Magazine, 1995, 37(1): 48-55.

[75] REZAIERLAK R, MANTEGHI M. Short-time matrix pencil method for chipless rfid detection applications[J]. IEEE Transactions on Antennas and Propagation, 2013, 61(5): 2801-2806.

[76] KALANSURIYA P, KARMAKAR N C, VITERBO E. On the detection of frequency-spectra-based chipless RFID using UWB impulsive interrogation[J]. IEEE Transactions on Microwave Theory and Techniques, 2012, 60(12): 4187-4197.

[77] BABAEIAN F, KARMAKAR N C. Time and frequency domains analysis of chipless RFID back-scattered tag reflection[J]. IoT, 2020, 1(1): 109-127.

[78] RAMOS A, PERRET E, RANCE O, et al. Temporal separation detection for chipless depolarizing frequency-coded RFID[J]. IEEE Transactions on Microwave Theory and Techniques, 2016, 64(7): 2326-2337.

[79] ALIASGARI J, KARMAKAR N C. Mathematical model of chipless RFID tags for detection improvement[J]. IEEE Transactions on Microwave Theory and Techniques, 2020, 68(10): 4103-4115.

[80] LECUN Y, BENGIO Y, HINTON G. Deep learning [J]. Nature, 2015, 521(7553): 436-444.

[81] QIN Z, YE H, LI G Y, et al. Deep learning in physical layer communications[J]. IEEE Wireless Communications, 2019, 26(2): 93-99.

[82] LI Z, LIU F, YANG W, et al. A survey of convolutional neural networks: analysis, applications, and prospects[J]. IEEE Transactions on Neural Networks and Learning Systems, 2022, 33(12): 6999-7019.

[83] SCHUSTER M, PALIWAL K K. Bidirectional recurrent neural networks[J]. IEEE Transactions on Signal Processing, 1997, 45(11): 2673-2681.

[84] GRAVES A. Supervised sequence labelling with recurrent neural networks[M]. Boston, MA, USA: Springer, 2012.

[85] BALDI P. Autoencoders, unsupervised learning, and deep architectures[C]//Proceedings of ICML Workshop on Unsupervised and Transfer Learning. Belmont: Microtome Publishing, 2011: 37-49.

[86] LIU Z, ZHANG S, LIU Q, et al. Wifi-diffusion: Achieving fine-grained wifi radio map estimation with ultra-low sampling rate by diffusion models[J]. IEEE Journal on Selected Areas in Communications, 2025.

[87] XU M, NIYATO D, ZHANG H, et al. Sparks of generative pretrained transformers in edge intelligence for the metaverse: Caching and inference for mobile artificial intelligence-generated content services [J]. IEEE Vehicular Technology Magazine, 2023, 18 (4): 35-44.

[88] XU M, NIYATO D, CHEN J, et al. Generative ai-empowered simulation for autonomous driving in vehicular mixed reality metaverses[J]. IEEE Journal of Selected Topics in Signal Processing, 2023, 17(5): 1064-1079.

[89] MAO Q, HU F, HAO Q. Deep learning for intelligent wireless networks: A comprehensive survey[J]. IEEE Communications Surveys & Tutorials, 2018, 20(4): 2595-2621.

[90] LIU X, ZHANG H, BIAN K, et al. Meta-backscatter: A new ISAC paradigm for battery-free internet of things[J]. IEEE Communications Magazine, 2024, 62(9): 106-112.

[91] CHEN H, LIU X, ZHANG H, et al. Energy-efficient multi-tag meta-backscatter systems for battery-free internet of things[C]//Proceedings of IEEE Global Communications Conference (GLOBECOM). Piscataway: IEEE Press, 2025.

[92] XU Z, ZHANG H, SONG L. Dual-functional internet of meta-material things: Joint sensing and communication design[J]. IEEE Communications Letters, 2023, 27(10): 2862-2866.

[93] LIU F, CUI Y, MASOUROS C, et al. Integrated sensing and communications: Toward dual-functional wireless networks for 6G and beyond[J]. IEEE Journal on Selected Areas in Communications, 2022, 40(6): 1728-1767.